ELSEVIER

Chemical Engineering and Processing 39 (20000) 433–440

Chemical Engineering and Processing

www.elsevier.com/locate/cep

Rise velocity of single circular-cap bubbles in two-dimensional beds of powders and liquids

R. Krishna *, J.M. van Baten, M.I. Urseanu, J. Ellenberger

Department of Chemical Engineering, University of Amsterdam, Nieuwe Achtergracht 166, 1018 WV Amsterdam, The Netherlands

Accepted 23 November 1999

Abstract

An expression for the rise velocity of single circular-cap gas bubbles in two-dimensional (2D) beds consisting of powders or liquids is developed with the aid of experimental data and computational fluid dynamics. Experiments were performed in a two-dimensional rectangular column of width $D_T = 0.3$ m by injecting air bubbles in fluidised beds of silica (mean particle size, $d_p = 38$ μm) and polystyrene (mean particle size, $d_p = 570$ μm) and in water. The rise velocity of single gas bubbles in the size range $d_b = 0.015$–0.12 m were found to decrease significantly with increasing ratio of bubble diameter to bed width, d_b/D_T. Computational fluid dynamics simulations of single gas bubbles rising in water, carried out using the volume-of-fluid (VOF) method, showed good agreement with experiment and were used to develop a common expression for the rise velocity of single gas bubbles in gas–solid fluidised beds and bubble columns. The 2D circular-cap bubble rise velocity is found to ~ 10–30% lower than that of a 3D spherical-cap bubble having the same equivalent diameter.

Keywords: Bubble rise velocity; Two-dimensional; Computational fluid dynamics; Volume-of-fluid; Wall effect

1. Introduction

Experimental work to study bubbling behaviour and hydrodynamics is often carried out using two-dimensional rectangular gas-solid fluidised beds [1,2] and gas–liquid bubble columns [3]. In order to be able to translate the information from 2D beds to columns of cylindrical cross-section, it is important to be able to inter-relate the single bubble rise velocity in these two column configurations.

For a single gas bubble of equivalent diameter d_b rising in a liquid inside a cylindrical column of diameter D_T, Collins [4] gives the following expression for the rise velocity (see also Clift et al. [5], Davidson et al. [6], Fan and Tsuchiya [7], Wallis [8]) wherein a scale factor SF is introduced into the classical Davies–Taylor [9] relation:

$$V_b = 0.71\sqrt{gd_b}(SF) \tag{1}$$

The expression derived empirically by Collins [4] for the scale factor SF is

$$SF = 1 \quad \text{for } \frac{d_b}{D_T} < 0.125$$

$$SF = 1.13\exp\left(-\frac{d_b}{D_T}\right) \quad \text{for } 0.125 < \frac{d_b}{D_T} < 0.6$$

$$SF = 0.496\sqrt{D_T/d_b} \quad \text{for } \frac{d_b}{D_T} > 0.6 \tag{2}$$

Eqs. (1) and (2) are valid for spherical cap bubbles rising in inviscid flow; this condition is satisfied when the Eötvos number, Eö > 40 [5]. The same expression is valid for a single bubble rising in a gas–solid fluidised bed [1,5–7]. Bubbles in a smaller diameter column tend to rise slower than bubbles in a larger diameter column due to the restraining effects of the column walls. Such wall effects can be expected to diminish with increasing column diameter. A corresponding set of relations for bubbles, of circular-cap shape, rising in 2D columns is not available in the literature.

The experimental data of Pyle and Harrison [10] for 2D gas bubbles in rectangular gas–solid fluid beds of Ballotini, sand and iron shots lie significantly below

* Corresponding author. Tel.: +31-20-5257007; fax: +31-20-5255604.

E-mail address: krishna@chemeng.chem.uva.nl (R. Krishna).

0255-2701/00/$ - see front matter
PII: S0255-2701(99)00108-7

that calculated from the Davies–Taylor–Collins relation for 3D spherical cap bubbles; see Fig. 1. Pyle and Harrison [10] correlated their experimental data with the following expression

$$V_b = 0.48\sqrt{gd_b} \quad (3)$$

where d_b is the diameter of a bubble having the same area as the 2D bubble. The experimental data of Pyle and Harrison [10], however, shows considerable scatter and their developed relation in Eq. (3) is not very convincing.

There have been some attempts to develop fundamental relationships for the rise velocity of 2D circular cap bubbles. Collins [11] modelled the effect of the constraining walls in terms of the known potential flow due to a doublet in a uniform stream between two walls and applied the classical Davies–Taylor analysis to obtain the rising velocity in terms of the radius of curvature of the nose. The expression for the rise velocity is given in terms of the radius of curvature of the nose and the half-width of the channel. This work was extended by Hills [12], who replaced the doublet by a separated source and sink to give an ellipse-like closed streamline. Garabedian [13] has derived the theoretical slug flow limit, valid for narrow columns. Gera and Gautam [14] have attempted a theoretical analysis of the rise of 2D gas bubble in a gas–solid fluidised bed as a parallel to the Davies–Taylor [9] treatment but the influence of the wall is not taken into account.

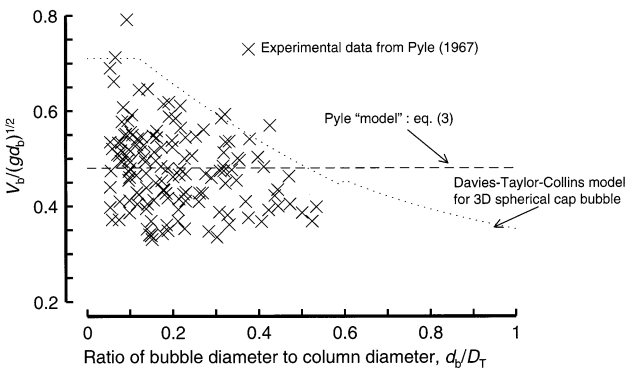

Fig. 1. Experimental data of Pyle and Harrison [10] for rise velocity of gas bubbles in 2D rectangular columns as a function of bubble diameter to column diameter. Also shown in the figure are the calculations from the Davies–Taylor–Collins model for single spherical-cap bubbles.

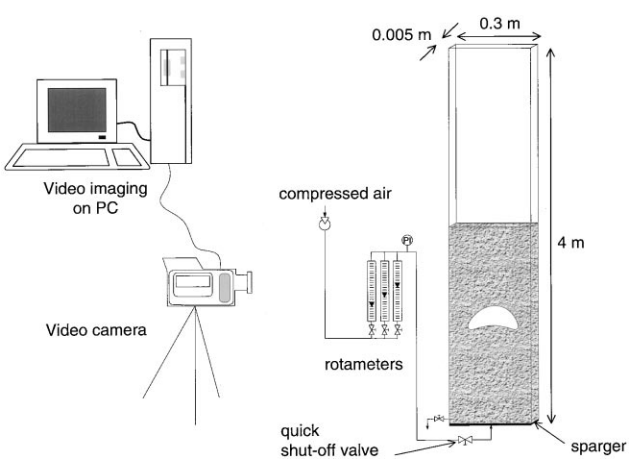

Fig. 2. The experiment set-up for measurement of rise velocities of single gas bubbles in water and in fluidized beds of silica and polystyrene.

The aim of the present paper is to develop an expression for the rise velocity of single circular-cap gas bubble in 2D columns, in terms of the equivalent bubble diameter, to parallel Eqs. (1) and (2). Both experimental data and computational fluid dynamics (CFD) are used to develop this expression.

2. Experimental

Single bubble rise velocities were measured in a rectangular column made up of two parallel glass plates of 0.3 m width and 4 m height; see Fig. 2. The distance between the glass plates was 5 mm. A sintered plate distributor (of 50 μm pore size) ensured uniform gas distribution at the bottom. Additionally, there was provision to inject gas bubbles via a central tube of 2 mm diameter. The column was filled with either water, porous silica particles (Geldart A powder with skeleton density = 2100 kg m^{-3}; pore volume = 1.05 ml g^{-1}; particle size distribution, d_p: 10% < 27 μm; 50% < 38 μm; 90% < 47 μm) or porous polystyrene particles (Geldart B powder with particle density = 1073 kg m^{-3}; particle size distribution, d_p: 10% < 480 μm; 50% < 570 μm; 90% < 630 μm). For measurements with powders, the bed was maintained under minimum fluidisation conditions before injecting single gas bubbles through the central nozzle. The bubble trajectories were recorded on video at 25 frames per second using the image capturing set-up described in an earlier study [3]. Accurate determination of the bubble size and rise velocity was obtained by frame-by-frame analysis of the captured video images. The bubble sizes used in the air–water experiments ranged from 0.017–0.10 m. A circular cap shape was obtained in all cases. Bubbles larger than 0.12 m were found to be unstable. The bubble size range used in the air–silica experiments were in the range 0.01–0.03 m; larger sized bubbles were unstable. In the air–polystyrene experiments the bubble sizes ranged from 0.06 to 0.16 m.

The experimental data on the rise velocities in water, silica and polystyrene are shown in Fig. 3. The experimental data lie about 10–30% below the values calculated from the Davies–Taylor–Collins model. Based on the experimental data alone, it is difficult to set up a relation to parallel Eqs. (1) and (2) because the range of

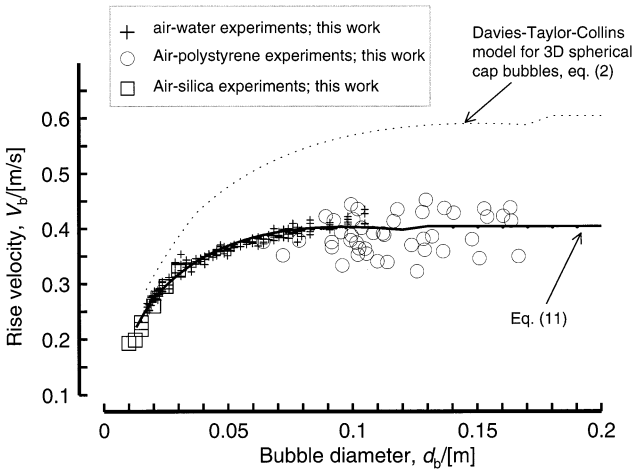

Fig. 3. Comparison of experimental data on rise velocity in air–solid and air–water systems with the Davies–Taylor–Collins relationship for spherical cap bubbles. Also shown in the figure is the curve according to Eq. (11) derived in this work for 2D circular cap bubbles.

d_b/D_T values in the experiments is restricted to below 0.5. To develop a reliable correlation would require us to carry out experiments in rectangular columns of varying width. In an earlier experimental study on the rise velocity of spherical cap bubbles in liquids, we had carried out measurements in cylindrical columns of diameters 0.05, 0.1, 0.174 and 0.63 m (Krishna et al. [15]). In this study, we had established the validity of the Davies–Taylor–Collins relations in Eqs. (1) and (2) to describe the rise velocity of single spherical-cap bubbles for systems conforming to the criterion Eö > 40. Furthermore, we had demonstrated that the volume-of-fluid (VOF) method is able to provide an accurate description of the bubble rise velocity. Our strategy in the present study is to use the VOF technique as supplement to our experimental data in the 2D rectangular column in our efforts to develop a relation to parallel the Davies–Taylor–Collins model.

3. Volume-of-fluid simulations

The VOF model [15–22] resolves the transient motion of the gas and liquid phases using the Navier–Stokes equations, and accounts for the topology changes of the gas–liquid interface induced by the relative motion between the dispersed gas bubble and the surrounding liquid. The finite-difference VOF model uses a donor–acceptor algorithm, originally developed by Hirt and Nichols [17], to obtain, and maintain, an accurate and sharp representation of the gas–liquid interface. The VOF method defines a fractional volume or 'colour' function $c(\mathbf{x}, t)$ that indicates the fraction of the computational cell filled with liquid. The colour function varies between 0, if the cell is completely occupied by gas, and 1, if the cell consists only of the liquid phase. The location of the bubble interface is tracked in time by solving a balance equation for this function:

$$\frac{\partial c(\mathbf{x}, t)}{\partial t} + \nabla \cdot (\mathbf{u} c(x, t) = 0 \tag{4}$$

The liquid and gas velocities are assumed to equilibrate over a very small distance and essentially $\mathbf{u}_k = \mathbf{u}$ for k = L, G at the bubble interface. The mass and momentum conservation equations can be considered to be homogenous:

$$\nabla \cdot (\rho \mathbf{u}) = 0 \tag{5}$$

$$\frac{\partial \rho \mathbf{u}}{\partial t} + \nabla \cdot (\rho \mathbf{u}\mathbf{u}) = -\nabla p - \nabla \cdot \tau + \rho \mathbf{g} + \mathbf{F}_{sf} \tag{6}$$

where p is the pressure, τ is the viscous stress tensor, $\mathbf{g}$ is the gravitational force. The density and viscosity used in Eqs. (6) and (7) are calculated from

$$\rho = \varepsilon_L \rho_L + \varepsilon_G \rho_G; \quad \mu = \varepsilon_L \mu_L + \varepsilon_G \mu_G \tag{7}$$

where ε_k denotes the volume fraction of the phase k = L, G. The continuum surface force model, originally proposed by Brackbill et al. [23], is used to model the force due to surface tension acting on the gas–liquid interface. In this model the surface tension is modelled as a body force $\mathbf{F}_{sf}$, that is non-zero only at the bubble interface and is given by the gradient of the colour function

$$\mathbf{F}_{sf} = \sigma \kappa(\mathbf{x}) \nabla c(\mathbf{x}, t) \tag{8}$$

where $\kappa(\mathbf{x})$ is the local mean curvature of the bubble interface:

$$\kappa(\mathbf{x}, t) = -\nabla \cdot \left(\frac{\mathbf{n}}{|\mathbf{n}|} \right) \tag{9}$$

where $\mathbf{n}$ is the vector normal to the bubble interface

$$\mathbf{n} = \nabla c(x, t) \tag{10}$$

The set of Eqs. (4)–(10) were solved using the commercial flow solver CFX 4.1c of AEA Technology, Harwell, UK. This package is a finite volume solver, using body-fitted grids. The grids are non-staggered and all variables are evaluated at the cell centres. An improved version of the Rhie-Chow [24] algorithm is used to calculate the velocity at the cell faces. The pressure–velocity coupling is obtained using the SIMPLEC algorithm [25].

Table 1 summarises the details of all the 2D simulations that were carried out using the parallel version of CFX 4.1c running on Silicon Graphics Power Challenge machine with six R8000 processors run in parallel. The simulations were carried out using a uniform 2D Cartesian coordinate grid with a grid size of 1 mm. The front of the 2D rectangular grid is formed by the

xz-plane. At the two walls, the no-slip boundary condition is imposed. The column is modelled as an open system, so the pressure in the gas space above the initial liquid column is equal to the ambient pressure (101.325 kPa). For the convective terms in the equations hybrid differencing was used. Upwind differencing was used for the time integration. The time step used in the simulations was 0.0004 s. To counteract excessive smearing of the liquid–gas interface by numerical diffusion, a surface sharpening routine was invoked. This routine identifies gas and liquid on the 'wrong' side of the interface, and moves it back to the correct side, while conserving volume of the respective phases. In order to avoid 'dissolution' of the bubble due to surface sharpening we found it necessary to ensure that each bubble area encompassed a few hundred cells. For simulation of the rise of spherical cap bubbles, typically found with sizes above 17 mm, a grid size of 1 mm was found to be adequately small; in this case the number of grid cells per bubble cross-section was in excess of 300. For all simulations reported here a bubble neither gained nor lost more than $\sim 10\%$ area during its rise. Animations of the simulations carried out to study the scale effects in 2D rectangular geometry can be viewed our web site http://ct-cr4.chem.uva.nl/cartesian/.

For all the simulations listed in Table 1 circular cap shaped bubbles were obtained. To give an indication of the required CPU time, the simulation of the rise of a 0.031 m diameter bubble for 0.5 s in a column of 0.3 m width and 0.5 m height, involving 150 000 grid cells, required ~ 9 days. Snapshots of a simulation of a typical 2D simulation of the rise of a 0.033-m bubble in a 0.1-m wide column are shown in Fig. 4. The total column was 0.5 m in height with a gas cap of 0.03 m at the top. As initial condition a semi-circular shaped bubble, of equivalent diameter 0.033 m, was placed near the bottom of the column. To ensure convergence in the initial period when the bubble 'adjusts' itself to its surrounding and begins its ascent, the following time stepping strategy was used: 50 steps at 5×10^{-5} s, 50 steps at 2.5×10^{-5} s, 50 steps at 5×10^{-5} s and 2000 steps at 4×10^{-4} s. For each time step about 40 iterations were typically required to obtain convergence of the governing equations. A bubble typically attains its terminal velocity after ~ 0.15 s from the start of the simulation. The bubble rise velocity was determined by a linear regression of the z-coordinates of the nose of the bubble during steady-rise. Fig. 5 compares the z-coordinates of the nose of 0.033 m bubbles rising in columns of 0.1 and 0.051 m diameters; this figure shows that the bubble rises faster in the wider column. The

Table 1
Results of two-dimensional VOF simulations in Cartesian geometry[a]

Bubble diameter, d_b (m)	Column diameter, D_T (m)	Grid size, Δx ($=\Delta z$) (mm)	Time step, Δt (s)	Rise velocity, V_b (m s^{-1})
0.020	0.4	1	0.0004	0.277
0.0203	0.6	1	0.0004	0.275
0.021	0.051	1	0.0004	0.16
0.031	0.3	1	0.0004	0.317
0.033	0.051	1	0.0004	0.163
0.0359	0.051	1	0.0004	0.1605
0.046	0.051	1	0.0004	0.168
0.033	0.1	1	0.0004	0.2235

[a] In all cases the gas phase was air ($\rho_G = 1.29$ kg m^{-3}, $\mu_G = 1.7 \times 10^{-5}$ Pa s) and the liquid was water ($\rho_L = 998$; $\mu_L = 10^{-3}$; $\sigma = 0.072$ N m^{-1}).

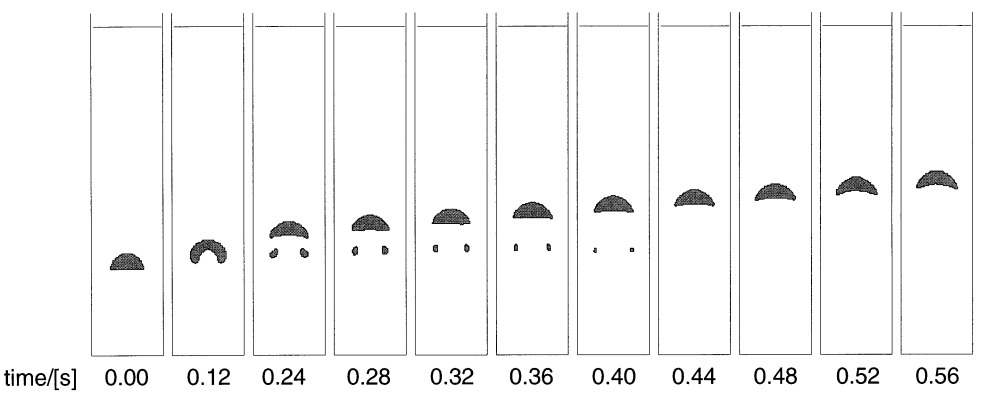

Fig. 4. Snapshots of VOF simulations of rise of a 0.033-m diameter air bubble in a column of 0.1 m width filled with water. Animations of this VOF simulations can be viewed on our web site http://ct-cr4.chem.uva.nl/cartesian.

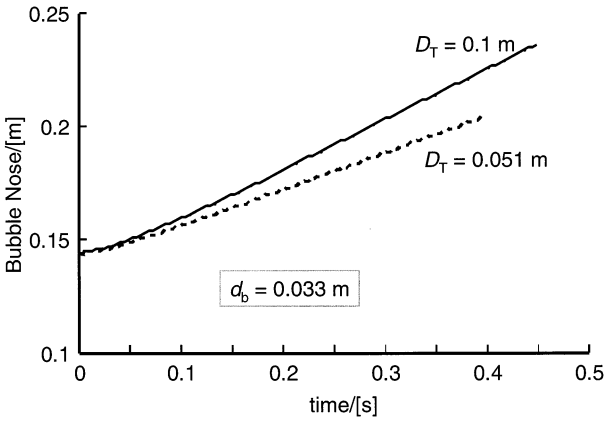

Fig. 5. Comparison of the rise trajectories of a 0.033-m diameter bubble rising in columns of 0.051 and 0.1 m width filled with water. Animations of these VOF simulations can be viewed on our web site http://ct-cr4.chem.uva.nl/cartesian.

reason for this is the restraining effect of the walls. Fig. 6 shows the computational snapshots for these two simulations. We notice that the 0.033-m bubble assumes a flatter shape in the 0.1-m wide column and is less influenced by the wall than the same bubble placed in a 0.051-m wide column. Put another way, the drag between the bubble and the liquid is higher in the column of smaller width due to the higher downward liquid velocity near the bubble.

The rise velocity data from VOF simulations were combined with our experimental data (air–water, air–silica, air–polystyrene) and regressed to obtain the following correlation:

$$V_b = 0.62\sqrt{gd_b}(SF)$$

$$SF = 1 \quad \text{for } \frac{d_b}{D_T} < 0.07$$

$$SF = 1.1\exp\left(-1.55\frac{d_b}{D_T}\right) \quad \text{for } 0.07 < \frac{d_b}{D_T} < 0.4$$

$$SF = 0.38\sqrt{D_T/d_b} \quad \text{for } \frac{d_b}{D_T} > 0.4 \qquad (11)$$

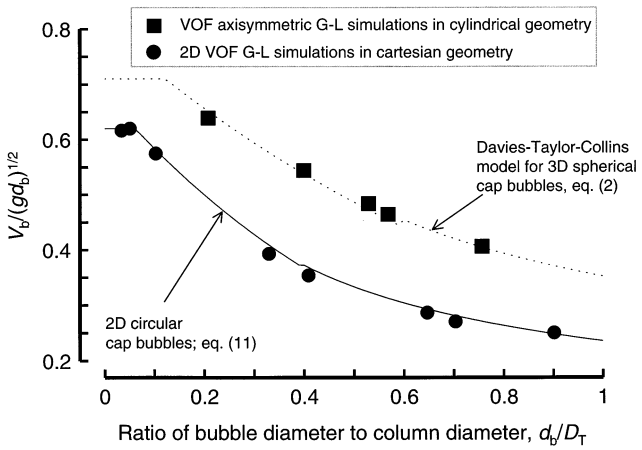

Fig. 7. Rise velocities determined from VOF simulations for air–water system are compared with the correlations given by eq (2) for 3D spherical cap bubbles and Eq. (11) for 2D circular cap bubble. For 3D spherical cap bubbles the VOF simulations were performed in cylindrical coordinates assuming axisymmetry; these simulations have been reported earlier by Krishna et al. [15].

Fig. 7 compares the calculations from Eq. (11) with VOF simulations. For comparison purposes, we have also plotted the Davies–Taylor–Collins model calculations (using Eqs. (1) and (2)), along with the VOF simulations for a 3D spherical cap bubble we had published earlier [15]. The rise velocity of a 2D circular cap bubble is ~ 10–30% lower when compared with a 3D spherical cap bubble having the same equivalent diameter. We also note from Eq. (11) that for narrow columns (slug flow) the value of the rise velocity is $V_b = 0.236\sqrt{gD_T}$ which matches closely with the value derived theoretically by Collins [11] (who gives $V_b = 0.23\sqrt{gD_T}$) and Garabedian [13] (who has derived $V_b = 0.238\sqrt{gD_T}$).

In order to provide further verification of the conclusion that the rise velocity of circular-cap bubbles in 2D gas–solid and gas–liquid systems is described by an identical relationship, we undertook to compare CFD simulations of a the formation and rise of a single gas bubble in a 2D rectangular gas–solid fluidised bed and in an identical bed filled with water. For simulation of

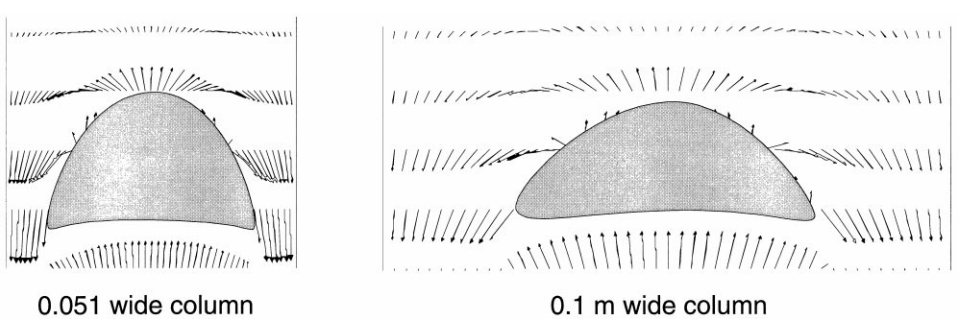

Fig. 6. Comparison of the snapshots of the VOF simulations of a 0.033-m diameter bubble rising in columns of 0.051 and 0.1 m width. Animations of these two VOF simulations can be viewed on our web site http://ct-cr4.chem.uva.nl/cartesian.

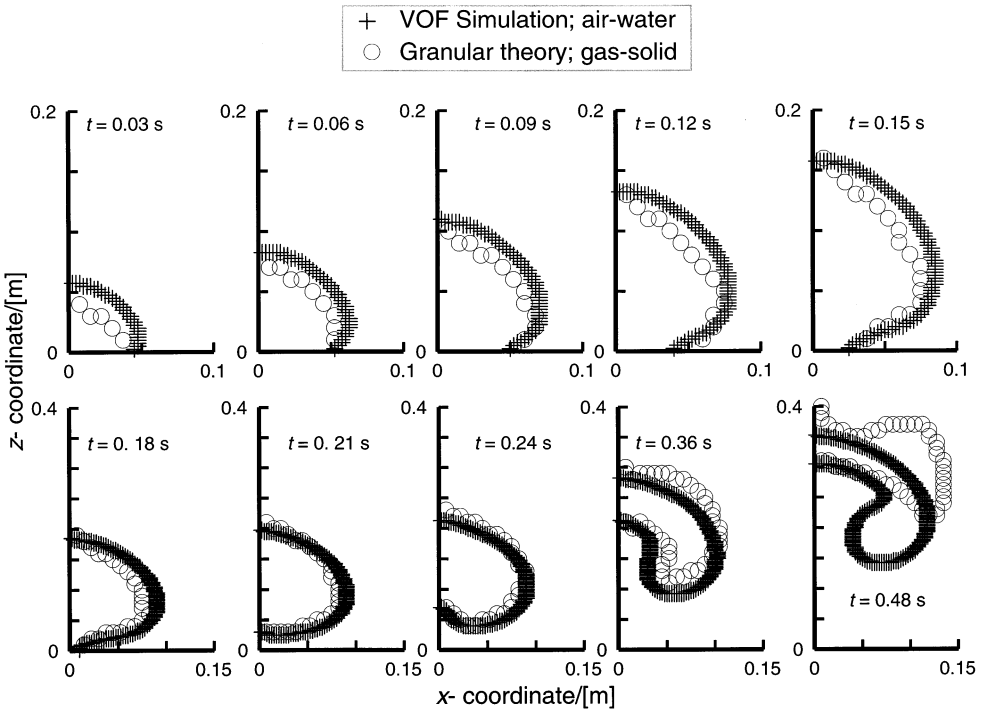

Fig. 8. Snapshots of the simulation of a formation of a gas bubble in a gas–solid fluidised bed of powder and water carried out respectively with the granular theory and VOF technique. The bubble contours are drawn at various time steps. Note the change in the scales between the upper and bottom rows. For a gas–solid system the contours of a bubble are defined by the requirement that the voidage is greater than 0.85. Animations of these simulations can be viewed on our web site http://ct-cr4.chem.uva.nl/analogies.

a gas–solid system, the kinetic theory of granular flow is well-established [26–35]. The variety of formulations of the kinetic theory of granular flow differ mainly with respect to the description of (a) the solids shear viscosity, (b) the drag coefficient describing the interaction between the solid particles and the gas phase, and (c) the radial distribution function g_0 at contact between the gas and the solid. A comparison of the various treatments is given by Van Wachem et al. [35].

We carried out axisymmetric granular theory simulations of a gas jet entering a 0.57 m wide rectangular fluid bed consisting of a powder of mean particle size of 500 μm with a skeletal density of 2660 kg m^{-3}. The gas jet enters the bed with a velocity of 10 m s^{-1} and is maintained for 0.18 s from the start of gas injection. The system geometry is the same as the one used by Kuipers et al. (1992). The granular theory was implemented within the CFX 4.1c code of AEA Technology, Harwell using a variety of models for the drag coefficient, radial distribution function g_0 and the solids shear viscosity. Snapshots of the bubble formation and rise are shown in Fig. 8 for a particular choice of models (Ergun [36], Wen and Yu [37] drag relation, Gidaspow [29] g_0 function and Syamlal and O'Brien [32] solids shear viscosity relation). Also shown in Fig. 8 are VOF simulations of an air–water system under identical conditions. The equivalence of the bubble formation and rise phenomena is evident in the initial stages. For a gas–solid system there is no surface tension and the bubble break-up phenomenon is different; this is evident towards the latter stages of bubble rise (see snapshot at $t = 0.48$ s). Animations of the granular theory and VOF simulations can be viewed on our web site http://ct-cr4.chem.uva.nl/analogies, wherein further computational details are available. The time trajectories of the nose of the bubble in Fig. 8 are compared in Fig. 9. It is clear that the rise velocity is identical in the initial stage of bubble rise. The agreement between the VOF simulations of G–L systems with the granular theory shown in Figs. 8 and 9 is

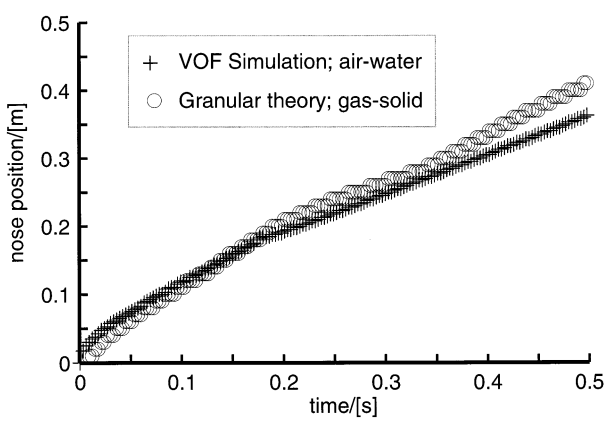

Fig. 9. Comparison of the rise trajectories of the bubble in the granular and VOF simulations shown in Fig. 8.

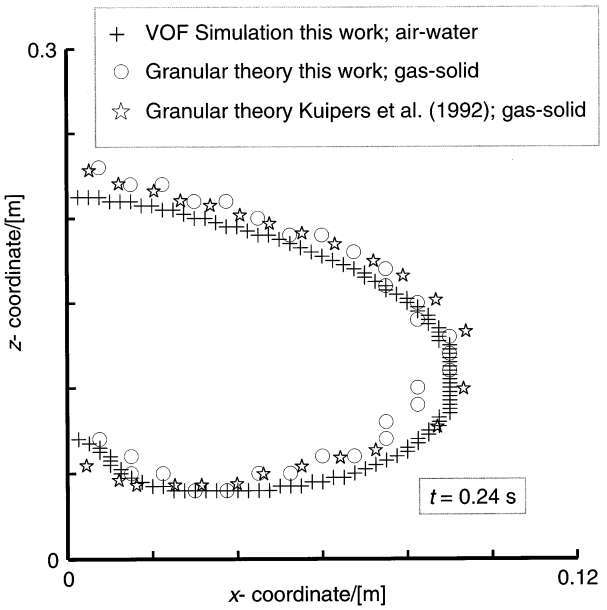

Fig. 10. Comparison of bubble contours calculated our specific choice of sub-models (Ergun [36], Wen and Yu [37] drag relation, Gidaspow [29] g_0 function and Syamlal and O'Brien [32] solids shear viscosity relation) with the original simulation of Kuipers et al. [31] for a gas–solid fluid bed. Also shown are VOF simulations for the same system. The simulations are for gas–solid fluid bed of 0.57 m width at time $t = 0.24$ s after gas injection.

not specific to the choice of the chosen sub-models with respect to drag, g_0 and solids shear viscosity. Other choices of the sub-models lead to substantially same results and conclusions. To emphasise this, we have compared in Fig. 10 our particular choice of sub-models used in Fig. 8 with the granular theory calculations of Kuipers et al. [31].

The results in Figs. 8 and 9 underline the analogies in the bubble rise phenomena in powders and liquids and go some way in explaining the reason behind a common rise velocity relationship in Eq. (11) which has been developed in this work.

4. Conclusions

The following conclusions can be drawn:

(1) The rise velocity of circular-cap bubbles in powders and liquids decreases with increasing ratio of bubble diameter to column width, d_b/D_T. This wall-effect is described quantitatively by the empirical relation in Eq. (11). Eq. (11) is the 2D analogue of the Davies–Taylor–Collins relation describing the rise velocity of spherical cap bubbles.

(2) VOF simulations for air–water systems in 2D rectangular columns provide some insight into the physics underlying the wall-effects. The downward flowing liquid near the walls influences the drag experienced by the bubbles; this drag reduces as the bubble is further removed from the walls.

(3) The rise velocity for air bubbles in water obtained from VOF simulations agree very well with our experimental data.

(4) The rise velocity of a 2D circular cap bubble is ~ 10–30% lower when compared with a 3D spherical cap bubble having the same equivalent diameter.

(5) A comparison of simulations using the granular theory for gas–solid fluid beds and VOF simulations for air–water systems underlines the analogies in bubble formation and bubble rise in gas–solid and gas–liquid systems.

Acknowledgements

The Netherlands Organisation for Scientific Research (NWO) is gratefully acknowledged for providing financial assistance to J.M. van Baten.

Appendix A. Nomenclature

$c(\mathbf{x}, t)$	colour function, dimensionless
d_b	equivalent bubble diameter (m)
d_p	particle diameter (m)
D_T	column diameter (m)
Eö	Eötvös number, $g(\rho_L-\rho_G)d_b^2/\sigma$
$\mathbf{F}_{sf}$	surface tension force (N m^{-3})
g	acceleration due to gravity (9.81 ms^{-2})
g_0	radial distribution function, dimensionless
$\mathbf{n}$	vector normal to the interface, dimensionless
p	pressure (N m^{-2})
SF	scale correction factor, dimensionless
t	time (s)
$\mathbf{u}$	velocity vector (m s^{-1})
V_b	rise velocity of the bubble (m s^{-1})
$\mathbf{x}$	position coordinate (m)
x	x-coordinate in cartesian geometry (m)
z	distance coordinate along height of column (m)

Greek letters

ε	volume fraction of phase, dimensionless
$\kappa(\mathbf{x})$	curvature of bubble interface, dimensionless
μ	viscosity of phase (Pa s)
ρ	density of phases (kg m^{-3})
σ	surface tension of liquid phase (N m^{-1})
τ	viscous stress tensor (N m^{-2})

Subscripts

b	referring to bubble
G	referring to gas phase
L	referring to liquid phase

p referring to particle
T tower or column

References

[1] D. Geldart (Ed.), Gas Fluidization Technology, Wiley, New York, 1986.
[2] R.F. Mudde, H.B.M. Schulte, H.E.A. van den Akker, Analysis of a bubbling 2-D gas-fluidized bed using image-processing, Powder Technol. 81 (1994) 149–159.
[3] J.W.A. De Swart, R.E. Van Vliet, R. Krishna, Size, structure and dynamics of 'large' bubbles in a 2-D slurry bubble column, Chem. Eng. Sci. 51 (1996) 4619–4629.
[4] R. Collins, The effect of a containing cylindrical boundary on the velocity of a large gas bubble in a liquid, J. Fluid Mech. 28 (1967) 97–112.
[5] R. Clift, J.R. Grace, M.E. Weber, Bubbles, Drops and Particles, Academic Press, San Diego, 1978.
[6] J.F. Davidson, D. Harrison, R.C. Darton, R.D. LaNauze, The two-phase theory of fluidization and its application to chemical reactors, in: L. Lapidus, N.R. Amundson (Eds.), Chemical Reactor Theory, A Review, Prentice-Hall, Englewood Cliffs, NJ, 1977, pp. 583–685.
[7] L.S. Fan, K. Tsuchiya, Bubble Wake Dynamics in Liquids and Liquid–Solid Suspensions, Butterworth–Heinemann, Boston, MA, 1990.
[8] G.B. Wallis, One-Dimensional Two-Phase Flow, McGraw-Hill, New York, 1969.
[9] R.M. Davies, G.I. Taylor, The mechanics of large bubbles rising through extended liquids and through liquids in tubes, Proc. R. Soc. Lond. A200 (1950) 375–390.
[10] D.L. Pyle, D. Harrison, The rising velocity of bubbles in two-dimensional fluidized beds, Chem. Eng. Sci. 22 (1967) 531–535.
[11] R. Collins, A simple model of the plane gas bubble in a finite liquid, J. Fluid Mech. 22 (1965) 763–771.
[12] J.H. Hills, The two-dimensional elliptical cap bubble, J. Fluid Mech. 68 (1975) 503–512.
[13] P.R. Garabedian, On steady-state bubbles generated by Taylor instability, Proc. R. Soc. A 241 (1957) 423–431.
[14] D. Gera, M. Gautam, Bubble rise velocity in two-dimensional fluidized beds, Powder Technol. 84 (1995) 283–285.
[15] R. Krishna, M.I. Urseanu, J.M. Van Baten, J. Ellenberger, Rise velocity of a swarm of large gas bubbles in liquids, Chem. Eng. Sci. 54 (1999) 171–183.
[16] E. Delnoij, J.A.M. Kuipers, W.P.M. van Swaaij, Computational fluid dynamics applied to gas–liquid contactors, Chem. Eng. Sci. 52 (1997) 3623–3638.
[17] C.W. Hirt, B.D. Nichols, Volume of fluid (VOF) method for the dynamics of free boudaries, J. Comput. Phys. 39 (1981) 201–225.
[18] R. Krishna, J.M. Van Baten, Simulating the motion of gas bubbles in a liquid, Nature 398 (1999) 208.
[19] R. Krishna, J.M. van Baten, Rise characteristics of gas bubbles in a 2D rectangular column: VOF simulations vs. experiments, Int. Comm. Heat Mass Transfer 26 (1999) 965–974.
[20] R. Krishna, M.I. Urseanu, J.M. Van Baten, J. Ellenberger, Wall effects on the rise of single gas bubbles in liquids, Int. Comm. Heat Mass Transfer 26 (1999) 781–790.
[21] A. Tomiyama, I. Zun, A. Sou, T. Sakaguchi, Numerical analysis of bubble motion with the VOF method, Nucl. Eng. Des. 141 (1993) 69–82.
[22] A. Tomiyama, A. Sou, H. Minagawa, T. Sakaguchi, Numerical analysis of a single bubble by VOF method, JSME Int. J. Ser. B 36 (1993) 51–56.
[23] J.U. Brackbill, D.B. Kothe, C. Zemarch, A continuum method for modelling surface tension, J. Comput. Phys. 100 (1992) 335–354.
[24] C.M. Rhie, W.L. Chow, Numerical study of the turbulent flow past an airfoil with trailing edge separation, AIAA J. 21 (1983) 1525–1532.
[25] J. Van Doormal, G.D. Raithby, Enhancement of the SIMPLE method for predicting incompressible flows, Numer. Heat Transfer 7 (1984) 147–163.
[26] A. Boemer, H. Qi, U. Renz, Eulerian simulation of bubble formation at a jet in a two-dimensional fluidized bed, Int. J. Multiphase Flow 23 (1997) 927–944.
[27] J. Ding, D. Gidaspow, A bubbling fluidization model using the kinetic theory of granular flow, AIChE J. 36 (1990) 523–538.
[28] L.S. Fan, C. Zhu, Principles of Gas–Solid Flows, Cambridge University Press, Cambridge, 1997.
[29] D. Gidaspow, Multiphase Flow and Fluidization — Continuum and Kinetic Theory Descriptions, Academic Press, San Diego, 1994.
[30] J.T. Jenkins, S.B. Savage, A theory for the rapid flow identical, smooth, nearly elastic spherical particles, J. Fluid Mech. 130 (1983) 187–202.
[31] J.A.M. Kuipers, K.J. van Duin, F.P.H. van Beckum, W.P.M. van Swaaij, A numerical model of gas fluidized beds, Chem. Eng. Sci. 47 (1992) 1913–1924.
[32] M. Syamlal, T.J. O'Brien, Computer simulation of bubbles in a fluidized bed, AIChE Symp. Ser. No. 270 85 (1989) 22–31.
[33] B.G.M. Van Wachem, J.C. Schouten, R. Krishna, C.M. Van den Bleek, Eulerian simulations of bubbling behaviour in gas–solid fluidized beds, Comput. Chem. Eng. 22 (1998) S299–S306.
[34] B.G.M. Van Wachem, J.C. Schouten, R. Krishna, C.M. Van den Bleek, Validation of the Eulerian simulated dynamic behaviour of gas–solid fluidised beds, Chem. Eng. Sci. 54 (1999) 2141–2149.
[35] B.G.M. Van Wachem, J.C. Schouten, R. Krishna, C.M. Van den Bleek, J.L. Sinclair, CFD modeling of gas–solid flow: qualititative and quantitative analysis of the various treatments, Proceedings of the 3rd ASME/JSME Joint Fluids Engineering Conference, 18–23 July, 1999, San Francisco, CA.
[36] S. Ergun, Fluid flow through packed columns, Chem. Eng. Prog. 48 (1952) 89–94.
[37] C.Y. Wen, Y.H. Yu, Mechanics of fluidization, AIChE J. Symp. Ser. 62 (1966) 100–111.